Available online at www.sciencedirect.com

SciVerse ScienceDirect

Ceramics International 39 (2013) 4701–4705

CERAMICS INTERNATIONAL

www.elsevier.com/locate/ceramint

Short communication

Excellent DC aging behavior of ZnO–Pr $_6O_{11}$–CoO–Cr_2O_3–Y_2O_3 ceramics modified with Tb_4O_7

Choon-W. Nahm*

Semiconductor Ceramics Laboratory, Department of Electrical Engineering, Dongeui University, Busan 614-714,Republic of Korea

Received 6 October 2012; accepted 3 November 2012
Available online 16 November 2012

Abstract

The microstructure, electrical properties, and aging behavior of the ZnO–Pr $_6O_{11}$–CoO–Cr_2O_3–Y_2O_3 varistor ceramics modified with Tb_4O_7 were investigated. The microstructure consisted of ZnO grain and an intergranular layer (Pr-, Y-, and Er-rich phases) as a secondary phase. The increase in the amount of Tb_4O_7 decreased the average grain size from 8.0 to 4.6 μm and increased the sintered density from 5.72 to 5.82 g/cm^3. As the amount of Tb_4O_7 increased, the breakdown field increased significantly from 2886 to 6902 V/cm and the nonlinear coefficient increased from 32.5 to 40.3 at 0.75 mol%. The varistor ceramics added with 0.5 mol% Tb_4O_7 exhibited excellent stability by exhibiting −0.1% in the variation rate of the breakdown field and −0.3% in the variation rate of the nonlinear coefficient for aging stress state of 0.95 $E_{1\,mA}$/150 °C/24 h.

Keywords: B. Grain boundaries; C. Electrical properties; C. Aging behavior; E. Varistors

1. Introduction

ZnO-based varistors are a kind of electrical switching devices sensing a transient overvoltage. They act like an insulator before transient overvoltages are applied to system, whereas they act like a conductor as soon as they sense transient overvoltages. This behavior is entirely attributed to the distinctive microstructure in the ZnO-based varistor ceramics. They are made by sintering a pressed ZnO body containing minor components such as Bi_2O_3 (or Pr_6O_{11}), CoO, Cr_2O_3, MnO_2, etc. A sintered ZnO body consists of many ZnO grains and grain boundaries, which have an absolute effect on varistor properties in terms of microstructure and electrical viewpoint. ZnO varistor ceramics with strong nonlinear properties can be widely used to overvoltage protection systems from electronic circuits to electric power systems [1,3].

The majority of commercial ZnO varistor ceramics are modified with Bi_2O_3. However, they have a few drawbacks because of the high volatility and reactivity of Bi_2O_3 during liquid sintering due to their relatively low melting point [4]. High reactivity of Bi_2O_3 may also destroy the multi-layer structure of chip varistors and deteriorate the surge-absorption capabilities because many secondary phases decrease the effective grain boundary area. For this reason, ZnO–Pr $_6O_{11}$-based ceramics have been studied [5–11].

ZnO–Pr $_6O_{11}$-based varistor ceramics are being studied to further enhance varistor properties and stability against various stresses, such as DC-accelerated aging stress and impulse stress [12–19]. Nahm and Shin [13,14,16], Nahm and Shin [14,16] and Nahm [15,17–19] reported that ZnO–Pr $_6O_{11}$–CoO–Cr_2O_3 (called ZPCC)-based varistor ceramics modified with rare earth oxides (Er, Y, Dy, La, etc.) have good nonlinear properties and high electrical stability against various stresses. These varistor ceramics have only five components. To develop varistor ceramics for wide band applications with a higher performance, it is necessary to study the effects of the new combination of additives on nonlinear properties and stability against the stress. A study on ZnO–Pr $_6O_{11}$-based varistor ceramics consisting of six components is rare yet [20].

*Tel.: +82 51 890 1669; fax: +82 51 890 1664.
E-mail address: cwnahm@deu.ac.kr

0272-8842/$ - see front matter © 2012 Elsevier Ltd and Techna Group S.r.l. All rights reserved.
http://dx.doi.org/10.1016/j.ceramint.2012.11.009

In this study the effect of Tb_4O_7 addition on the microstructure, electrical properties, and aging behavior of the ZnO–Pr $_6O_{11}$–CoO–Cr_2O_3–Y_2O_3–Tb_4O_7 varistor ceramics consisting of six components was investigated and some new results in terms of ceramic densification and electrical stability were obtained.

2. Experimental procedure

The ceramic composition used in this experiment is (97.5–x) mol% ZnO, 0.5 mol% Pr_6O_{11}, 1.0 mol% CoO, 0.5 mol% Cr_2O_3, 0.5 mol% Y_2O_3, and x mol% Tb_4O_7 (x=0.25, 0.5, 0.75, 1.0). Raw materials were mixed by ball milling with zirconia balls and acetone in a polypropylene bottle for 24 h. The mixture calcined at 750 °C for 2 h was pressed into discs 10 mm in diameter and 1.5 mm in thickness at a pressure of 80 MPa. The disk-shaped pellets were sintered for 1 h at 1350 °C. The sintered pellets were lapped and polished to 1.0 mm thickness. The final pellets were roughly 8 mm in diameter and 1.0 mm in thickness. Silver paste was coated on both faces of the pellets and the electrodes were formed by heating it at 600 °C for 10 min. Finally, after soldering the lead wire to both electrodes, the samples were packaged by dipping them into a thermoplastic resin powder.

The surface microstructure was examined by a scanning electron microscope (SEM, Hitachi S2400, Japan). The average grain size (d) was determined by the lineal intercept method, given by $d=1.56L/MN$, where L is the random line length on the micrograph, M is the magnification of the micrograph, and N is the number of grain boundaries intercepted by the lines [21]. The crystalline phases were identified by an X-ray diffractometer (XRD, Rigaku D/max 2100, Shibuya-Ku, Tokyo, Japan) with CuK_α radiation. The sintered density (ρ) was measured using a density determination kit (238490) attached to a balance (Mettler Toledo AG 245, Mettler Toledo International Inc., Greifensee, Switzerland).

The electric field–current density (E–J) characteristics were measured using a V–I source (Keithley 237). The breakdown field ($E_{1\ mA}$) was measured at 1.0 mA/cm^2, and the leakage current density (J_L) was measured at 0.8 $E_{1\ mA}$. In addition, the nonlinear coefficient (α) is defined by the empirical law $J=KE^\alpha$, where J is the current density, E is the applied electric field, and K is a constant. α was determined in the current density range of 1.0–10 mA/cm^2, where $\alpha=(\log J_2-\log J_1)/(\log E_2-\log E_1)$, and E_1 and E_2 are the electric fields corresponding to $J_1=1.0$ mA/cm^2 and $J_2=10$ mA/cm^2, respectively.

The DC-accelerated aging stress test was performed under four continuous conditions; the 1st stress: 0.85 $E_{1\ mA}$/115 °C/24 h, the 2nd stress: 0.90 $E_{1\ mA}$/120 °C/24 h, the 3rd stress: 0.95 $E_{1\ mA}$/125 °C/24 h, and the 4th stress: 0.95 $E_{1\ mA}$/150 °C/24 h.

The leakage current was monitored at intervals of 1 min during stressing using a high voltage source-measure unit (Keithley 237). The degradation rate coefficient (K_T) was calculated from the expression $I_L=I_{Lo}+K_Tt^{1/2}$ [22], where I_L is the leakage current at stress time (t), and I_{Lo} is I_L at t=0. After the respective stresses, the E–J characteristics were measured at room temperature.

3. Results and discussion

Fig. 1 shows the SEM micrographs of the samples modified with Tb_4O_7. Seemingly, surface morphology shows uniform grain sizes. The average grain size (d) decreased in the order of 8.0, 7.7, 5.2, and 4.7 μm due to increasing secondary phases with an increase in the amounts of Tb_4O_7. It can be seen that Tb_4O_7 restricts the

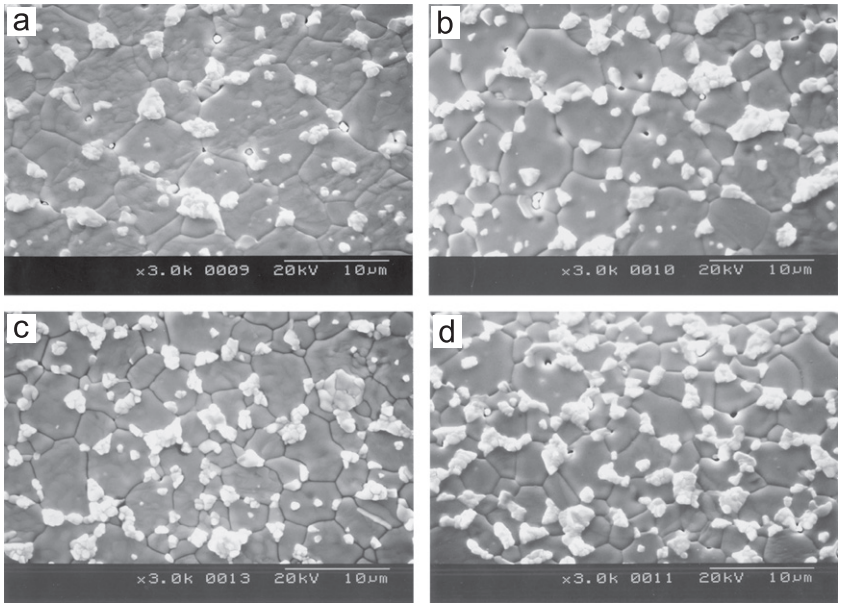

Fig. 1. SEM micrographs of the samples modified with Tb_4O_7. (a) 0.25 mol% (b) 0.5 mol% (c) 0.75 mol% (d) 1.0 mol%.

grain growth because of the segregation or/and precipitation at grain boundaries. The microstructure consisted of ZnO grain as a primary phase and an intergranular layer as a secondary phase. The XRD patterns indicated in Fig. 2 revealed the presence of Pr_6O_{11}-, Y_2O_3-, and Tb_4O_7-rich intergranular layer as minor secondary phases. The sintered density (ρ) increased in the order of 5.72, 5.76, 5.79, and 5.82 g/cm^3 (5.78 g/cm^3 in pure ZnO) with an increase in the amount of Tb_4O_7. Therefore, the densification of the samples is greatly enhanced by the addition of Tb_4O_7, compared with the samples with no Tb_4O_7 [5–20].

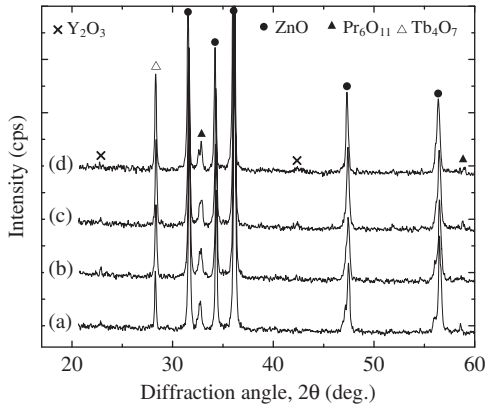

Fig. 2. XRD patterns of the samples modified with Tb_4O_7: (a) 0.25 mol%, (b) 0.5 mol%, (c) 0.75 mol%, and (d) 1.0 mol%.

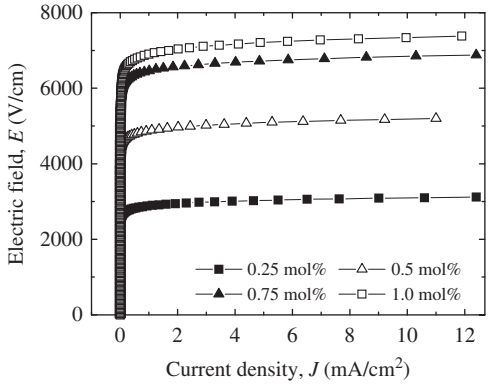

Fig. 3. *E–J* characteristics of the samples modified with Tb_4O_7.

Fig. 3 shows the *E–J* characteristics of the samples modified with Tb_4O_7. The curves are divided into non-conduction states as current-off and conduction states as current-on . This is considered as a nonlinear property. The Tb_4O_7 shifted the electric field curves to upper field strengths. Therefore, it can be forecasted that Tb_4O_7 addition has a strong effect on the *E–J* characteristics. The breakdown field ($E_{1\,mA}$), nonlinear coefficient (α), and leakage current density (J_L) obtained from *E–J* characteristic curves are indicated in Table 1. The $E_{1\,mA}$ increased from 2886 to 6902 V/cm with an increase in the amount of Tb_4O_7. The samples relatively provide a high breakdown field (close to 5000 V/cm or more) per unit thickness beyond 0.5 mol% in the amount of Tb_4O_7. It is obvious that this is very effective for high voltage varistors with a compact size. In general cases, the $E_{1\,mA}$ is directly related to the number of grain boundaries in accordance with ZnO grain size. When the breakdown voltage per grain boundary is in the range of 2–4 V/gb, the increase of $E_{1\,mA}$ as in this experiment is attributed to the increase of grain boundaries due to the decrease of grain size. As a result, the $E_{1\,mA}$ is significantly affected by the average grain size with an increase in the amount of Tb_4O_7.

The nonlinear coefficient (α) increased from 32.5 to 40.3 up to 0.75 mol% with an increase in the amount of Tb_4O_7. Further increase caused α to decrease to 37 at 1.0 mol%. Obviously, it can be seen that Tb_4O_7 has a significant effect

Table 1
E–J characteristic parameters after DC-accelerated aging stress for the samples modified with Tb_4O_7.

Tb_4O_7 amount (mol%)	Stress state	K_T (μA h$^{-1/2}$)	$E_{1\,mA}$ (V/cm)	%Δ$E_{1\,mA}$	α	%Δα	J_L (μA/cm^2)	%ΔJ_L
0.25	Initial	–	2886	0	32.5	0	3.6	0
	1st	3.8	2879	−0.2	32.0	−1.5	6.1	69.4
	2nd	0.1	2882	−0.1	32.3	−0.6	5.6	55.5
	3rd	0.4	2880	−0.2	32.2	−0.9	6.6	83.3
	4th	−18.3	2878	−0.1	32.4	−0.3	10.7	197.2
0.5	Initial	–	4875	0	37.3	0	1.5	0
	1st	−0.2	4876	0	37.3	0	2.0	33.3
	2nd	0.1	4876	0	37.2	−0.3	3.6	140.0
	3rd	−1.3	4874	0	37.2	−0.3	5.6	273.3
	4th	−32.3	4876	0	37.2	−0.3	4.6	206.7
0.75	Initial	–	6462	0	40.3	0	7.1	0
	1st	−1.5	6464	0	40.2	−0.3	11.2	57.7
	2nd	1.6	6458	−0.1	40.1	−0.5	16.3	129.6
	3rd	Thermal runaway						
1.0	Initial	–	6902	0	37.0	0	17.3	0
	1st	−0.5	6881	−0.3	37.2	0.5	19.9	15.0
	2nd	1.7	6871	−0.4	36.9	−0.3	23.5	35.8
	3rd	Thermal runaway						

on the nonlinear properties based on the change of α. The behavior of α with the amount of Tb_4O_7 will be related to the electronic barrier height caused by the electronic states at the grain boundaries due to Tb ions. The Tb_4O_7 will vary the density of the interface states by the transport of the Tb ions or other defect ions toward the grain boundary. Therefore this explanation indicates that the α can change due to the influence of Tb_4O_7. The J_L decreased to 1.5 μA/cm^2 up to 0.25 mol% with an increase in the amount of Tb_4O_7. Further increase in the amount of Tb_4O_7 increased it to 17.3 μA/cm^2 at 1.0 mol%. Therefore, it can be seen that the leakage current density can be obtained at a proper amount of Tb_4O_7. As a result, it is clear that the values of α and J_L were strongly affected by the amount of Tb_4O_7.

Fig. 4 shows the leakage current behavior at various DC-accelerated aging stresses for the samples modified with Tb_4O_7. The samples added with 0.75 and 1.0 mol% Tb_4O_7 exhibited high stability at the second stress (0.90 $E_{1\,mA}$/120 °C/24 h). However, they exhibited a thermal runaway at the third stress (0.95 $E_{1\,mA}$/125 °C/24 h). It is assumed that the thermal runaway of the samples modified with 0.75 and 1.0 mol% Tb_4O_7 is attributed to a high leakage current density. In general, a sintered density and leakage current have a severe effect on lasting stability. A low sintered density decreases the number of conduction paths, and eventually leads to the concentration of current. Furthermore, a high leakage current will lead to high joule heat loss and again joule heat will increase the leakage current. By the way, in the case of this experiment, the leakage current is likely to contribute greatly to the thermal runaway. On the other hand, the samples modified with 0.25 mol% and 0.5 mol% Tb_4O_7 exhibited a much higher stability, compared with the samples explained previously. This is attributed to a lower leakage current as well as a high sintered density. The stability of the varistors can be estimated by the degradation rate coefficient (K_T), which indicates the degree of aging. This is the slope of the leakage current for the stress time. In general, lower K_T values indicate greater stability, whereas it is not absolute estimation degree for stability. On the whole, the K_T of the sample modified with 0.5 mol% Tb_4O_7 is smaller than that of the sample modified with 0.25 mol% Tb_4O_7. In particular, they exhibited a negative creep of leakage current at most of the stress conditions. The sample modified with 0.25 mol% Tb_4O_7 exhibited a negative creep of leakage current as $-18.3\ \mu A\ h^{-1/2}$ in K_T value at the fourth stress (0.94 $E_{1\,mA}$/150 °C/24 h). The samples modified with 0.5 mol% Tb_4O_7 exhibited the lowest K_T value, which is $K_T = -32.3\ \mu A\ h^{-1/2}$ at the fourth stress (0.94 $E_{1\,mA}$/150 °C/24 h). It was confirmed that the resistance against the DC-accelerated aging stress is greatly affected by the amount of Tb_4O_7.

The *E–J* characteristic parameters, such as the variation rates of the breakdown field (%$\Delta E_{1\,mA}$), nonlinear coefficient (%Δα), and leakage current (%ΔJ_L) after applying the DC-accelerated aging stress, are summarized in Table 1. The samples modified with 0.25 mol% and 0.5 mol% Tb_4O_7 exhibited a low characteristic variation of −0.1% and 0.1% in %$\Delta E_{1\,mA}$, respectively, and −0.9% and −0.3% in %Δα, respectively after the fourth stress (0.95 $E_{1\,mA}$/150 °C/24 h). Based on %$\Delta E_{1\,mA}$ and %Δα, it is clear that the sample modified with 0.5 mol% Tb_4O_7 is more stable than the sample modified with

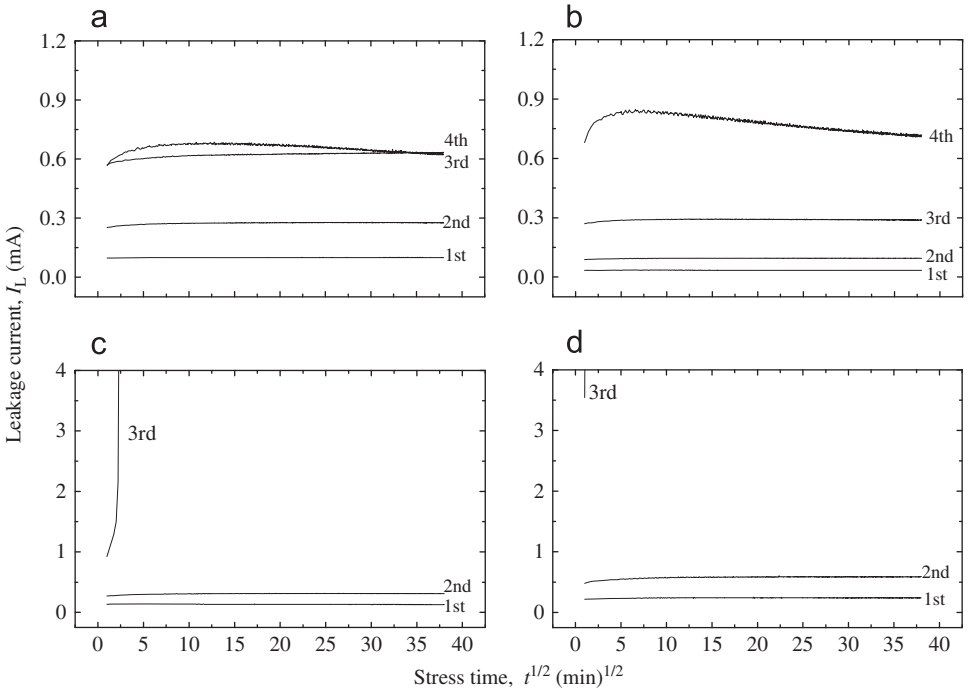

Fig. 4. Behavior of leakage current at applying various stresses for the samples modified with Tb_4O_7. (a) 0.25 mol% (b) 0.5 mol% (c) 0.75 mol% (d) 1.0 mol%.

0.25 mol% Tb_4O_7. The $\%\Delta J_L$ for both samples has very high variation, compared with $\%\Delta E_{1\,mA}$ and $\%\Delta\alpha$ after applying the fourth stress. However, the leakage current of the sample modified with 0.5 mol% Tb_4O_7 is only 4.6 $\mu A/cm^2$ after applying the fourth stress. This sample showed a much higher stability than any other ZnO–Pr $_6O_{11}$-based varistor ceramics as well as the samples with no Tb_4O_7 reported previously [12–20]. This is the most important point, which must be emphasized in this study. It is obviously confirmed that the ZnO–0 .5 Pr_6O_{11}–1.0 CoO–0 .5 Cr_2O_3–0.5 Y_2O_3–0.5 Tb_4O_7 (all in mol%) varistor ceramics sintered at 1350 °C exhibited the highest stability among varistor ceramics reported previously.

4. Conclusions

The effect of Tb_4O_7 addition on varistor properties, and aging behavior of the ZnO–Pr $_6O_{11}$–CoO–Cr_2O_3–Y_2O_3 ceramics were investigated. The addition of Tb_4O_7 resulted in a denser microstructure and increased the average grain size. The addition of Tb_4O_7 noticeably increased the breakdown field, and the nonlinear coefficient up to 0.75 mol%. The varistor ceramics added with 0.5 mol% Tb_4O_7 exhibited an excellent stability by exhibiting -0.1% in the variation rate of the breakdown field and -0.3% in the variation rate of the nonlinear coefficient for aging stress of 0.95 $E_{1\,mA}$/150 °C/24 h. These varistor ceramics may be applied to various fields, with a nonlinear coefficient close to 40 and a high breakdown field close to 5000 V/cm.

References

[1] L.M. Levinson, H.R. Philipp, Zinc oxide varistor–a review, American Ceramic Society Bulletin 65 (1986) 639–646.

[2] T.K. Gupta, Application of zinc oxide varistor, Journal of the American Ceramic Society 73 (1990) 1817–1840.

[3] J. Wong, Microstructure and phase transformation in a highly non-ohmic metal oxide varistor ceramic, Journal of Applied Physics 46 (1975) 1653–1659.

[4] Y.S. Lee, T.Y. Tseng, Phase identification and electrical properties in ZnO-glass varistors, Journal of the American Ceramic Society 75 (1992) 1636–1640.

[5] K. Mukae, K. Tsuda, I. Nagasawa, Non-ohmic properties of ZnO–rare earth metal oxide–Co $_3O_4$ Ceramics, Japanese Journal of Applied Physics 16 (1977) 1361–1368.

[6] K. Mukae, Zinc oxide varistors with praseodymium oxide, American Ceramic Society Bulletin 66 (1987) 1329–1331.

[7] H.K. Varma, K.P. Kumar, K.G.K. Warrier, A.D. Damodaran, Effect of K_2O on the sintered microstructure of praseodymium-doped ZnO varistors, Journal of Materials Science Letters 8 (1989) 974–976.

[8] A.B. Alles, V.L. Burdick, The effect of liquid-phase sintering on the properties of Pr6O11-based ZnO varistors, Journal of Applied Physics 70 (1991) 6883–6890.

[9] A.B. Alles, R. Puskas, G. Callahan, V.L. Burdick, Compositional effects on the liquid-phase sintering of praseodymium oxides-based zinc oxides varistors, Journal of the American Ceramic Society 76 (1993) 2098–2102.

[10] Y.-S. Lee, K.-S. Liao, T.-Y. Tseng, Microstructure and crystal phases of praseodymium in zinc oxide varistor ceramics, Journal of the American Ceramic Society 79 (1996) 2379–2384.

[11] C.-W. Nahm, The nonlinear properties and stability of ZnO–Pr $_6O_{11}$–CoO–Cr_2O_3–Er_2O_3 ceramic varistors, Materials Letters 47 (2001) 182–187.

[12] C.-W. Nahm, B.-C. Shin, Effect of sintering temperature on electrical properties and stability of Pr6O11-based ZnO varistors, Journal of Materials Science-Materials in Electronics 13 (2002) 111–120.

[13] C.-W. Nahm, S. -B. Shin, M.-H. Min, Microstructure and electrical properties of Y_2O_3-doped ZnO–Pr $_6O_{11}$-based varistor ceramics, Materials Chemistry and Physics 82 (2003) 157–164.

[14] C.-W. Nahm, B.-C. Shin, Effect of sintering time on electrical properties and stability against DC accelerated aging of Y_2O_3-doped ZnO–Pr $_6O_{11}$-based varistor ceramics, Ceramics International 30 (2004) 9–15.

[15] C.-W. Nahm, Electrical properties and stability against DC accelerated aging stress of ZPCCE-based varistor ceramics, Journal of Materials Science-Materials in Electronics. 15 (2004) 29–36.

[16] C.-W. Nahm, B.-C. Shin, Effect of sintering time on electrical characteristics and DC accelerated aging behaviors of Zn–Pr –Co–Cr–Dy oxide-based varistors, Journal of Materials Science-Materials in Electronics. 16 (2005) 725–732.

[17] C.-W. Nahm, Effect of sintering temperature on nonlinear electrical properties and stability against DC accelerated aging stress of (CoO, Cr_2O_3, La_2O_3)-doped ZnO–Pr $_6O_{11}$-based varistors, Materials Letters 60 (2006) 3311–3314.

[18] C.-W. Nahm, Electrical properties and aging characteristics of terbium-doped ZPCC-based varistors, Materials Science and Engineering B 137 (2007) 112–118.

[19] C.-W. Nahm, Electrical behavior against current impulse in ZnO–Pr $_6O_{11}$-based varistor ceramics with terbium addition, Ceramics International 36 (2010) 1495–1501.

[20] C.-W. Nahm, Microstructure, electrical properties, and aging behavior of ZnO–Pr $_6O_{11}$–CoO–Cr_2O_3–Y_2O_3–Er_2O_3 varistor ceramics, Ceramics International 37 (2011) 3048–3054.

[21] J.C. Wurst, J.A. Nelson, Lineal intercept technique for measuring grain size in two-phase polycrystalline ceramics, Journal of the American Ceramic Society 55 (1972) 109–111.

[22] J. Fan, R. Freer, Deep level transient spectroscopy of zinc oxide varistors doped with aluminum oxide and/or silver oxide, Journal of the American Ceramic Society 77 (1994) 2663–2668.